# A Novel Stress Relaxation Modeling for Predicting the Change of Residual Stress During Annealing Heat Treatment

QIAN BAI, HENG FENG, LI-KUN SI, RAN PAN, and YI-QI WANG

Large tensile residual stresses generated during cold working processes could negatively affect the integrity and geometric accuracy of workpieces. The stress relief annealing is one of the fundamental issues in controlling the deformation of the cold-worked part. A novel residual stress relaxation model was proposed to predict the change of residual stress during the annealing process by considering the dislocation evolution mechanism and the plasticity theory. Copper workpieces were rolled with different rolling ratios and annealed under different heating temperatures and heating times. Hole-drilling experiments were conducted to measure the residual stresses for calibrating the proposed model. The calibrated model was then used to predict the change of residual stresses during annealing heat treatment. The results showed that the initial work hardening of workpieces had a great effect on the residual stress relaxation. Higher initial dislocation density hindered the residual stress relaxation during the annealing process. The results provided guidance on optimizing the annealing conditions for residual stress reduction.

https://doi.org/10.1007/s11661-019-05454-z
© The Minerals, Metals & Materials Society and ASM International 2019

## I. INTRODUCTION

RESIDUAL stress has drawn remarkable attention in the metal-forming and machining fields by affecting the integrity of workpieces.[1] During a cold working process, tensile residual stress is commonly induced into workpieces, which can undermine its fatigue life, machinability, and geometric accuracy.[2] Stress-relief annealing is widely applied to reduce this kind of residual stress by heating the workpiece below its recrystallization temperature, keeping at a suitable temperature, and then cooling, which converts residual elastic strain to permanent inelastic deformation.

Currently, many researches on characterizing and predicting the residual stress relaxation in stress-relief annealing have been conducted *via* empirical models[3–7] and classical creep models.[8–11] The empirical models are capable of describing the reduction of residual stresses when the workpieces are subjected to elevated temperatures after shot peening,[12] additive manufacturing,[5] and machining.[6,13] Most of the empirical models are based on the thermodynamic behaviors of the workpieces, such as Zener–Wert–Avrami equation,[6,7] in which heating temperature and activation energy play the most important roles. Some other empirical models are proposed in the forms of exponential functions and calibrated by experimental data.[5] These empirical models could efficiently predict the residual stresses after annealing but failed to explain the physical mechanism of the residual stress relaxation.

In addition to the empirical models, classic creep models have also been extensively studied for residual stress relaxation. It is believed that the internal stress-induced creep deformation prompts the residual stress relaxation.[11] Therefore, steady-state creep models have been applied for the annealing process with workpieces of shot peening,[8] welding,[9] and casting.[10] In these models, the initial work hardening of the workpieces is neglected. However, the extent of initial work hardening influences the stress relaxation curves,[14] which is difficult to be implemented in classic creep models. Moreover, physically based models describe the plastic flow of the material considering the interaction of dislocations, the recovery *etc*.[15] Some researchers have used elastic–viscoplastic self-consistent model,[16] creep plasticity model,[17] and Orowan equation[11] to describe the thermal relaxation of residual stresses. Nevertheless, in these approaches, the dislocation density evolution was considered as an internal state variable, and the

QIAN BAI, HENG FENG, LI-KUN SI, and YI-QI WANG are with the Key Laboratory for Precision and Non-traditional Machining Technology of Ministry of Education, Dalian University of Technology, Dalian 116024, P.R. China. Contact e-mail: wangyiqi@dlut.edu.cn RAN PAN is with the Beijing Aeronautical Manufacturing Technology Research Institute, Beijing 100024, P.R. China.

Manuscript submitted Feburary 11, 2019.
Article published online September 18, 2019

dislocation density was not measured or calculated explicitly.

Actually, dislocation density theories have been widely studied in static/dynamic recovery and recrystallization,[18] and in crystal plasticity.[19] Blum *et al.*[20–22] quantitated the dislocation density evolution by calculating the generation and annihilation of single and dipole dislocations, which provides a feasible method to study the effect of dislocation density evolution on the thermal relaxation of residual stresses.

Therefore, a novel residual stress relaxation model is proposed to predict the change of residual stress during the annealing process by considering the dislocation evolution mechanism and the plasticity theory, in which the initial hardening conditions are considered as well. Annealing experiments of cold-rolled copper workpieces are conducted. The hole-drilling method, combined with the electronic speckle pattern interferometry (ESPI), is used to measure the residual stresses before and after annealing. The proposed novel model is validated by annealing experiments and predicted the change of residual stress at different annealing parameters.

## II. MODEL DESCRIPTION

Stress-relief annealing, as a process transforming elastic residual strain to permanent inelastic strain, generally reduces the residual stresses induced by preceding processes without the change of the microstructure. A novel residual stress relation model is proposed by implemented inelastic strain rate, dislocation motion, and dislocation evolution for predicting the change of residual stress at different annealing temperatures and times.

### A. *Inelastic Strain Rate in Plasticity Theory*

In the proposed residual stress relaxation process for cold-rolled copper workpieces, the residual stress is determined by the residual elastic strain in the form of Hook's law: $\sigma = E\varepsilon_e$, where $E$ is the elastic modulus. Total strain ($\varepsilon_{\text{tot}}$), consisting of elastic strain ($\varepsilon_{\text{e}}$) and inelastic strain ($\varepsilon_{\text{ie}}$), remains constant. During the annealing process, the elastic strain transforms to inelastic strain with the increasing time[23]:

$$\varepsilon_{\text{tot}} = \varepsilon_{\text{e}} + \varepsilon_{\text{ie}} \quad [1]$$

$$\dot{\varepsilon}_{\text{e}} = -\dot{\varepsilon}_{\text{ie}} \quad [2]$$

where $\dot{\varepsilon}_{\text{e}}$ and $\dot{\varepsilon}_{\text{ie}}$ are elastic strain rate and inelastic strain rate, respectively.

The plasticity and strain hardening are controlled by dislocations gliding for the materials with high stacking fault energy, such as pure copper.[24] The effects of stacking fault on strain rate are ignored in this paper. Orowan's equation[20,25] was adopted to calculate the inelastic strain rate:

$$\dot{\varepsilon}_{\text{ie}} = \rho_{\text{m}} \bar{v} b / M \quad [3]$$

where $\rho_{\text{m}}$ is mobile dislocation density, $\bar{v}$ is average velocity of dislocation motion, $b$ is Burgers vector, and $M$ is Taylor factor. In order to determine the inelastic strain rate, it is necessary to calculate dislocation motion $\bar{v}$ and mobile dislocation density $\rho_{\text{m}}$, respectively.

### B. *Dislocation Motion*

Frost and Ashby[26] concluded the average velocity of dislocation motion as

$$\bar{v} = \beta b v \exp\left(-\frac{\Delta G}{KT}\right) \quad [4]$$

where $\beta$ is a dimensionless constant, $v$ is the Debye frequency, $K$ is the Boltzmann constant, $T$ is the heating temperature, and $\Delta G$ is the Gibbs free energy of activation to overcome the obstacles inside the grains, which can be expressed as

$$\Delta G = \Delta F \times \left(1 - \frac{\sigma}{\hat{\sigma}}\right) \quad [5]$$

where $\sigma$ is the residual stress caused by residual elastic strain. $\Delta F$ is the total energy required to overcome obstacles without external applied stresses.[15] $\hat{\sigma}$ is the slip resistance due to dislocation interaction and other obstacles, and it has a relation with dislocation density as[27,28]

$$\hat{\sigma} = \sigma_0 + \frac{k_{\text{HP}}}{\sqrt{d}} + \chi M G_{\text{s}} b \sqrt{\rho} \quad [6]$$

where $\sigma_0$, the initial slip resistance caused by short-range obstacles, *i.e.,* the lattice friction stress, depends on the solute density of alloying element. For pure copper without solution element, after cold rolling, the increased slip resistance $\hat{\sigma}$ is mainly attributed to the intersection of the dislocations. Therefore, the lattice friction stress $\sigma_0$ was considered negligible. $k_{\text{HP}}$ is the Hall–Patch coefficient, $d$ is the grain size, $\chi$ is a proportional factor, and $G_{\text{s}}$ is the shear modulus. The term of $\frac{k_{\text{HP}}}{\sqrt{d}}$ represents the Hall-Patch strengthening effect and can also be neglected when the grain size is comparatively large (around 500 $\mu$m). Kocks and Mecking[29] pointed out that the term of $\chi M G_{\text{s}} b \sqrt{\rho}$ represents the dislocation strengthening due to the interaction of the dislocations, and it is proportional to the root square of dislocation density $\rho$. Therefore, a higher initial dislocation density requires a larger stress to overcome the slip resistance $\hat{\sigma}$. Shear modulus $G_{\text{s}}$ is temperature dependent and is expressed as[26]

$$G_{\text{s}} = G_0 \left(1 + \frac{T - 300}{T_{\text{m}}}\right) \frac{T_{\text{m}}}{G_0} \frac{\text{d}G_{\text{s}}}{\text{d}T} \quad [7]$$

where the shear modulus $G_0$ of the pure copper is 42 GPa at 300 K, $\frac{T_{\text{m}}}{G_0}\frac{\text{d}G_{\text{s}}}{\text{d}T} = 0.54$ is the temperature dependence of modulus, and the melting temperature of the pure copper $T_{\text{m}}$ is 1356 K.

$\Delta F$ in Eq. [5] is the activation energy to overcome the obstacles without the externally applied stress, which is expressed as

$$\Delta F = \alpha G_s b^3 \quad [8]$$

where $\alpha$ is an index which indicates the initial hardening level, and it lies between 0.2 to 1 with regard to forest dislocation hardening.[26] Since the hardening index $\alpha$ is dependent on the initial hardening conditions, it is necessary to determine the value $\alpha$ for workpieces with different rolling ratios.

### C. *Dislocation Density Evolution*

The dislocation density is an important parameter for determining the inelastic strain rate in residual stress relaxation. Roters *et al.*[19] and Bertin *et al.*[30] divided the dislocation density rate $\dot{\rho}$ into two parts: the generation rate of dislocation caused by hardening $\dot{\rho}^+$, and the annihilation rate caused by thermal softening $\dot{\rho}^-$:

$$\dot{\rho} = \dot{\rho}^+ - \dot{\rho}^- \quad [9]$$

Eisenlohr and Blum[22] described the dislocation generation rate caused by hardening as

$$\dot{\rho}^+ = \dot{\varepsilon}_{ie}/b\Lambda^+ \quad [10]$$

where $\dot{\varepsilon}_{ie}$ is inelastic strain rate. $\Lambda^+$ is the free path of a dislocation in the form of:

$$\Lambda^+ = K_\Lambda \rho^{-0.5} \quad [11]$$

where $K_\Lambda$is a material constant varying according to different materials. In Blum's theory,[20–22] total dislocation $\rho$ consists of single dislocations $\rho_{sgl}$ and dipole dislocations $\rho_{dip}$, and the annihilation rate of total dislocations $\dot{\rho}^-$ is the sum of that of single dislocations $\dot{\rho}^-_{sgl}$and dipole dislocations $\dot{\rho}^-_{dip}$:

$$\rho = \rho_{sgl} + \rho_{dip} \quad [12]$$

$$\dot{\rho}^- = \dot{\rho}^-_{sgl} + \dot{\rho}^-_{dip} \quad [13]$$

where the single dislocations are commonly considered as the mobile dislocations, which indicates that $\rho_m = \rho_{sgl}$.[19]

The annihilation rates of single dislocations and dipole dislocations are calculated as

$$\dot{\rho}^-_{sgl} = (4M/b) \times \left(\dot{\varepsilon}_{ie} d_{dip} \rho_{sgl}/n_g\right) \quad [14]$$

$$\dot{\rho}^-_{dip} = \left(1 - \frac{6b}{d_{dip}}\right) \times \dot{\rho}^-_{sgl} - \frac{12M\dot{\varepsilon}_{ie}\rho_{dip}}{n_g} - \rho_{dip} \times \frac{4v_c}{d_{dip} - 6b} \quad [15]$$

where $d_{dip}$ is the shortest distance to form a dislocation dipole, $n_g$ is the number of active slip systems, and $v_c$ is the climbing velocity of dislocation motion. They are in the forms of

$$d_{dip} = \frac{M}{8\pi(1-\mu)} \frac{G_s b}{\sigma} \quad [16]$$

$$v_c = D\Omega\sigma_c/bK_b T \quad [17]$$

where $D$ is the self-diffusion coefficient, $K_b$ is the Boltzmann constant,$\mu$ is the ratio, and $\Omega$ is the atom volume.$\sigma_c$ is the climbing stress applied to dislocations during the dislocation motion:

$$\sigma_c + \sigma_D = \frac{G_s b}{2\pi(1-\mu)} \frac{2}{d_{dip} + 6b} \quad [18]$$

where $\sigma_D$ is the stress for dragging a cloud of solutes, which can be neglected for pure copper.

The constants used in the proposed residual stress relaxation model are listed in Table I. The annealing heating temperature $T$ and total heating time $t_{tot}$ were input to the model. Initial residual stresses $\sigma_{ini}$ were measured by the hole-drilling-ESPI method. Initial dislocation densities $\rho_{ini}$ were obtained from X-ray diffraction (XRD). The differential equations in the proposed model were calculated. The theoretical residual stress relaxation curves were obtained for a given value of $\alpha$. Then, the value of $\alpha$ was determined by minimizing the error $e(\alpha)$ between the calculated and experimental results, as shown in Figure 1. Finally, the theoretical model was used to predict the change of residual stress at different annealing temperatures and times.

## III. EXPERIMENTAL SETUP

### A. *Specimen Preparation*

Rounded pure copper plates (Cu + Ag ≥ 99.9 pct) from China Luoyang Copper, Ltd. with a diameter of 100 mm were cold-rolled by multiple passes with different rolling ratios. Then the workpieces were annealed afterward to study the residual stress relaxation. The rolling ratio is defined as the ratio of thickness reduction to the original thickness. The plates were rolled from $h_0$ = 12 mm to a final thickness of $h$ = 10, 8, and 6 mm (shown in Figure 1), respectively, *i.e.*, with 17, 33, and 50 pct rolling ratio (RR). The amount of rolling reduction for each pass was set as 0.2 mm. After each pass, the plates were turned over and rotated by 45 deg until the final thickness to ensure the uniform deformation in the whole plate. Due to the friction and the continuous local deformation, nonuniform plastic strain and thus residual stresses existed in the in-plane direction of the rolled copper plates. It is assumed that the differences between the initial hardening conditions and

**Table I. Parameters Used in the Theoretical Model**

| $b$ (nm) | $K_b$ (J K$^{-1}$) | $\chi$ | $M$ | $K_\Lambda$ |
|---|---|---|---|---|
| 0.256[26] | $1.38 \times 10^{-23}$[26] | 1[29] | 3.06[26] | 30[20] |
| $n_g$ | $D$ | $v$ (Hz) | $\Omega$ (m$^3$) | $\mu$ |
| 2[22] | $2.19 \times 10^{-23}$[21] | $10^{13}$[21] | $1.18 \times 10^{-29}$[21] | 0.34[26] |

residual stresses are negligible in workpieces with the same rolling parameters. Therefore, residual stresses at the same locations on two workpieces before and after annealing were measured to evaluate the stress relaxation. The location of hole drilling measurement, dislocation density measurement, and microhardness measurement were shown in Figure 2.

One set of the annealing experiments were conducted to calibrate the model and determine the hardening index $\alpha$. The workpieces with different RRs were isothermally annealed at a temperature of 300 °C for 10, 20, 30, and 60 minutes. The maximum principal residual stresses were measured and calculated by the hole-drilling method. The other set of annealing experiments were conducted to validate the model. The workpiece with 50 pct RR was isothermally heated at temperatures of 250 °C, 350 °C, and 400 °C for 30 minutes. The residual stresses after annealing were measured and compared with calculated values. The heating parameters used in the annealing experiments are listed in Table II.

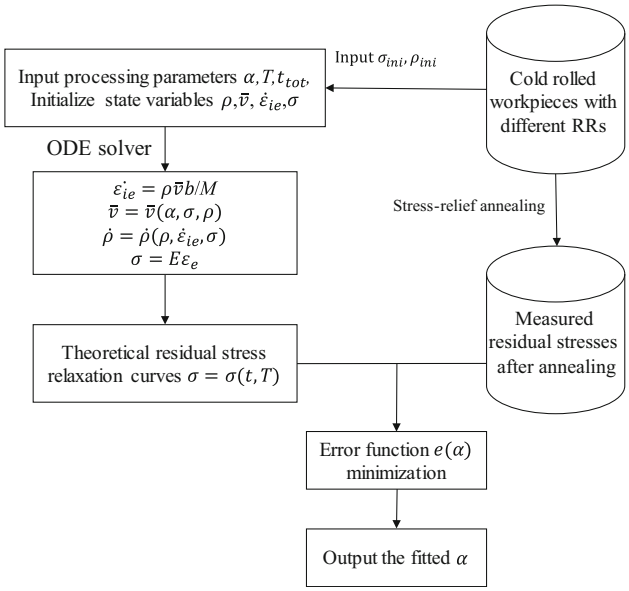


Fig. 1—Flowchart of the theoretical model for residual stress relaxation and determination of hardening index $\alpha$.

## B. *Residual Stress Measurement by the Hole-Drilling Method*

The hole-drilling method is one of the most common method for measuring the residual stress. The hole-drilling method can measure the residual stresses to a certain depth. Combined with full-field optical techniques such as electrical speckle pattern interferometry (ESPI), the hole-drilling method can provide an accurate residual stress measurement based on sufficient data around the holes.

The hole-drilling method combined with ESPI from StressTech, Ltd. was used to measure the residual stresses, as shown in Figure 3. ESPI system used a laser beam to capture images of the measurement surface before and after each drilling increment so that surface displacements due to the stress relief can be quantified. The coherent laser beam with a power of 20 mW used for illumination and generation of interference images could not influence the temperature or the microstructure of the specimens. The interference fringe images after hole drilling were recorded by the CCD camera, and the displacement was calculated according to the path length change in the illumination beam. Three measurements were conducted for each workpiece. The distance between the adjacent holes was 5 mm, to guarantee an unaffected stress relaxation region after hole drilling (Figure 2). A carbide end-mill with a diameter of 0.8 mm was used to drill the hole at a rotation speed of 30,000 rpm.

## C. *Dislocation Density Measurement via XRD Method*

XRD patterns were measured by using PANayltical Empyrean diffractometer to calculate initial dislocation densities of the rolled copper plates before annealing.

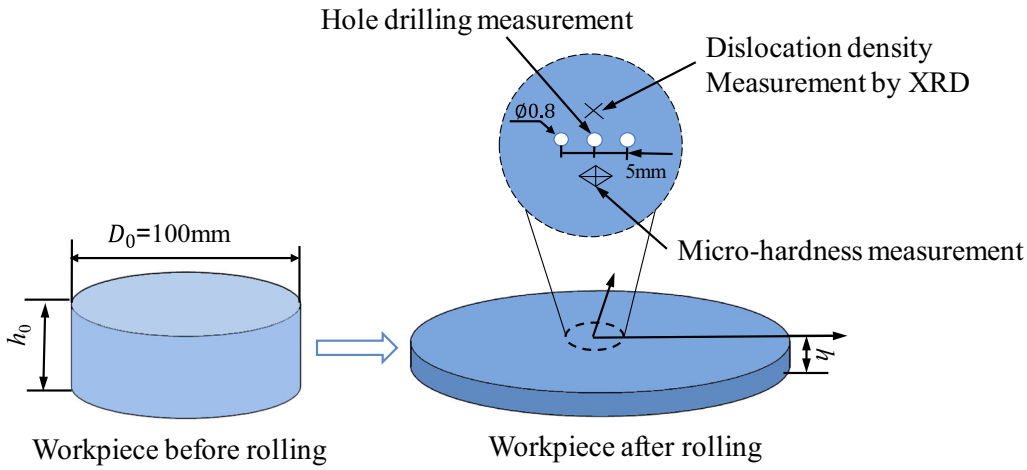


Fig. 2—Schematic for the cold-rolled workpieces and measurement locations.

The location of XRD measurement was shown in Figure 2. Bragg diffraction angle was selected from 20 to 130 deg and step length was 0.013 deg. Cobalt target was used in the diffraction as anode material with the tube tension of 40 kV and the current of 40 mA. The data collected in the measurement was analyzed using Jade 5.0 software. Williamson–Smallman method[31] was used to calculate the dislocation density from XRD diffraction patterns, which can be expressed as

$$\rho = 2\sqrt{3}\langle \varepsilon_m^2 \rangle^{1/2} / bD_c \quad [19]$$

where $D_c$ is the average crystallite size, and $\langle \varepsilon_m^2 \rangle^{1/2}$ is the root-mean-square of microstrain, which were obtained by means of Jade 5.0 software.

**Table II. Heating Parameters in the Annealing Experiments**

| Workpieces | Heating Time (min) | Heating Temperature (°C) |
|---|---|---|
| RR: 17, 33, and 50 Pct (Model Calibration) | 10 | 300 |
| | 20 | 300 |
| | 30 | 300 |
| | 60 | 300 |
| RR: 50 Pct (Model Validation) | 30 | 250 |
| | 30 | 350 |
| | 30 | 400 |

## IV. RESULTS AND DISCUSSIONS

### A. *Residual Stress and Dislocation Density Before Annealing*

Residual stresses before annealing were measured by the hole-drilling method combined with ESPI as shown in Figure 4. The residual stresses increased slightly from 120 to 180 MPa within the measuring depth when RRs increased. The residual stress after rolling can be

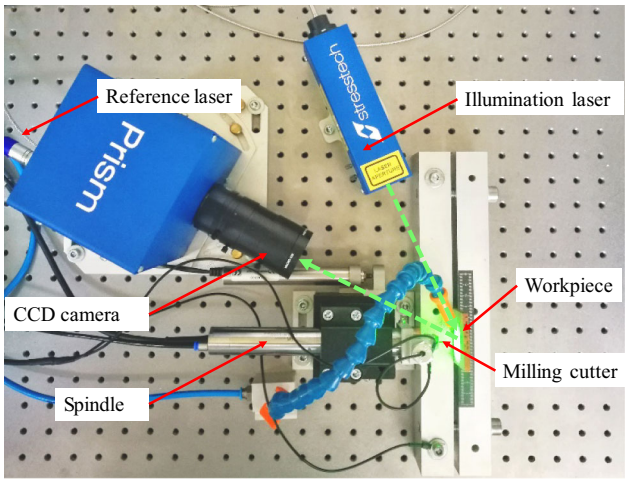


Fig. 3—An experimental setup of the hole-drilling-ESPI method.

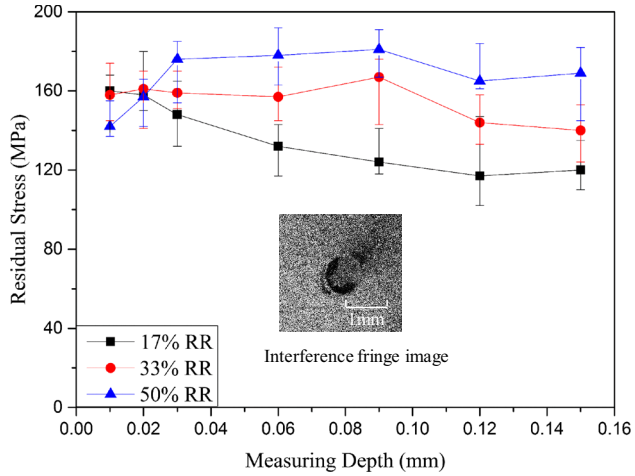


Fig. 4—Measurement of residual stresses before annealing.

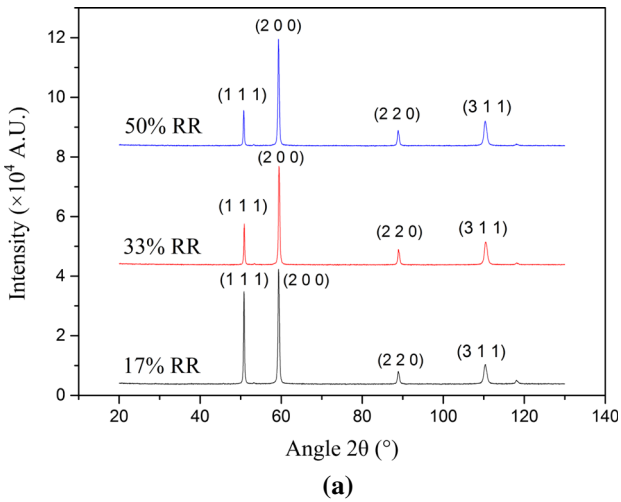


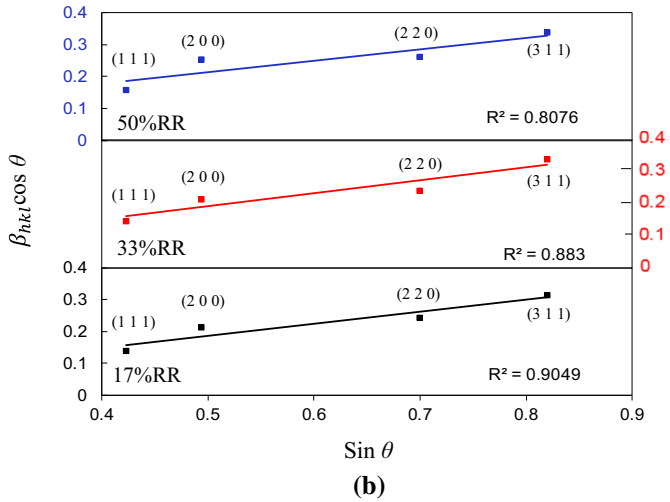


Fig. 5—(*a*) XRD patterns and (*b*) Williamson–Hall Plots of workpieces with different rolling ratios.

**Table III. XRD Data of Workpieces with Different Rolling Ratios and Annealed Workpiece**

| | $2\theta$, $FWHM$, $D_{hkl}$ for respective $hkl$ values | | | |
|---|---|---|---|---|
| Workpiece | 111 | 200 | 220 | 311 |
| 17 pct RR | | | | |
| $2\theta$ (deg) | 50.825 | 59.298 | 88.911 | 110.348 |
| FWHM | 0.176 | 0.281 | 0.362 | 0.562 |
| $D_{hkl}$ (nm) | 60.7 | 34.8 | 32.0 | 25.2 |
| 33 pct RR | | | | |
| $2\theta$ (deg) | 50.865 | 59.322 | 88.962 | 110.474 |
| FWHM | 0.185 | 0.285 | 0.356 | 0.605 |
| $D_{hkl}$ (nm) | 55.3 | 34.2 | 33.1 | 23.4 |
| 50 pct RR | | | | |
| $2\theta$ (deg) | 50.757 | 59.294 | 88.897 | 110.333 |
| FWHM | 0.196 | 0.322 | 0.371 | 0.601 |
| $D_{hkl}$ (nm) | 52.2 | 29.9 | 30.2 | 23.5 |
| Annealed (400 °C, 8 h) | | | | |
| $2\theta$ (deg) | 50.807 | 59.377 | 88.880 | 110.353 |
| FWHM | 0.088 | 0.134 | 0.119 | 0.127 |
| $D_{hkl}$ (nm) | > 100 | > 100 | > 100 | > 100 |

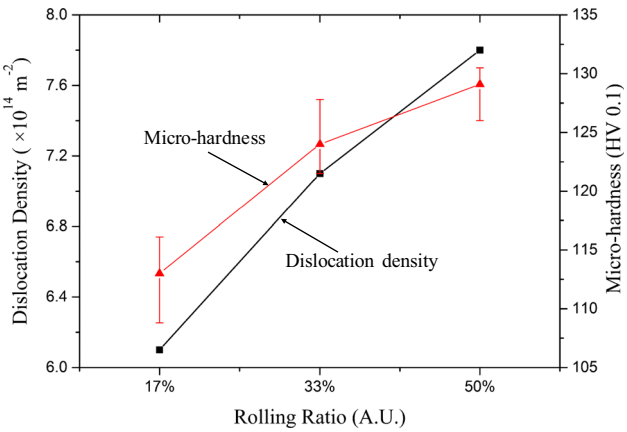


Fig. 6—Effects of rolling ratio on the dislocation density and microhardness before annealing.

considered to be evenly distributed within the measuring depth. Therefore, the average value of the maximum principal residual stresses was used to calibrate the theoretical model.

The diffraction patterns of XRD for workpieces with 17, 33 and 50 pct RR are shown in Figure 5(a). The Williamson-Hall plots are conducted to check the strain anisotropy before calculating the dislocation densities.[32] Another workpiece was annealed as a standard specimen to eliminate the instrumental broadening effect of XRD. The detailed information of each peak profile is listed in Table III. The results of linear fitting of $\sin\theta - \beta_{hkl}\cos\theta$ for different workpieces are presented in Figure 5(b), where $\beta_{hkl}$ is the corrected full width at half maximum ($FWHM$) for each peak. According to the good linear fitting results obtained under different RRs, the copper workpieces present a good strain isotropic property, and thus strain anisotropy is negligible.

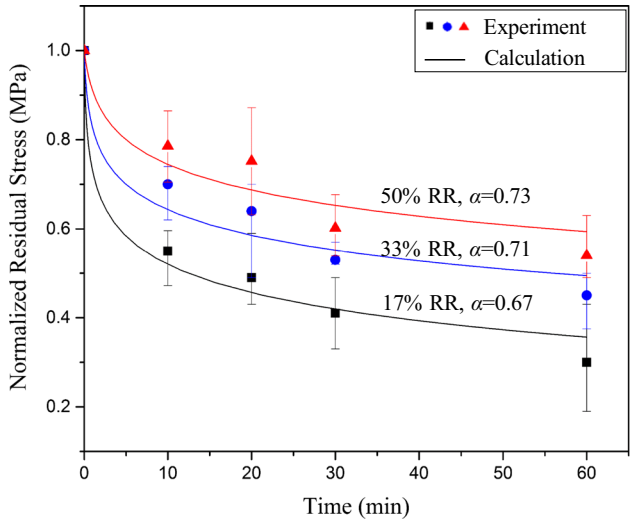


Fig. 8—Measured and calculated residual stresses with the fitted α after annealing at 300 °C.

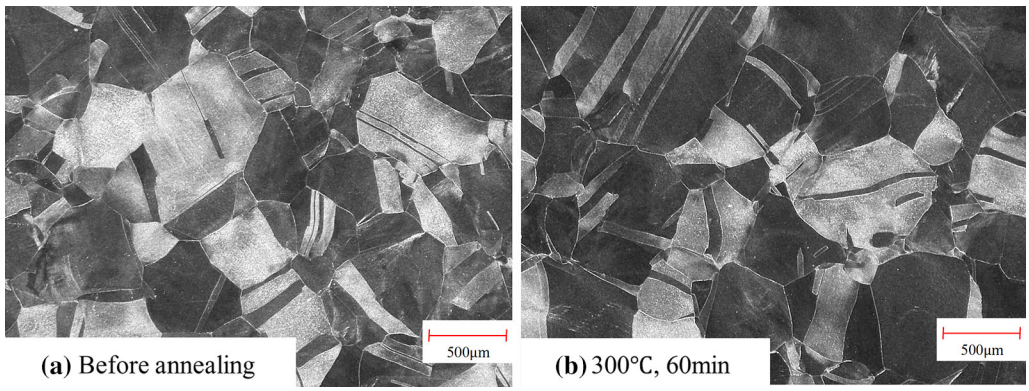


Fig. 7—Microstructures of workpieces with 50 pct RR: (*a*) before and (*b*) after annealing at 300 °C for 60 min.

Based on Eq. [19], the dislocation density for cold-rolled workpieces was calculated. As shown in Figure 6, when the RR increased from 17 to 50 pct, the dislocation density increased from $6.1 \times 10^{14}$ to $7.8 \times 10^{14}$ $m^{-2}$, and the hardness increased from 112 HV0.1 to 129 HV0.1. The increase of microhardness was consistent with that of dislocation density, which indicated that the hardening level was higher when the RR was larger.

## B. *Model Calibrations*

In order to calibrate the theoretical model, workpieces with different RRs were isothermally annealed at the temperature of 300 °C. The heating time was 10, 20, 30, and 60 minutes, respectively. The microstructures of workpieces with 50 pct RR before and after annealing at 300 °C for 60 minutes are presented in Figure 7. The grain size before annealing was about 500 $\mu$m (Figure 7(a)) and remained almost unchanged after annealing (Figure 7(b)). Recrystallization temperature is dependent on the initial grain size, deformation condition, annealing temperature, and time.[33] In this study, a relatively larger initial grain size 500 $\mu$m was used, and thus the recrystallization temperature was higher than the published literature.[34] From the microstructure observation, no obvious recrystallization or grain growth occurred after annealing for 60 minutes at 573 K. It is deduced that only residual stress relief occurred during the annealing. Therefore, the theoretical model, which ignored the microstructure evolution, is applicable to simulate the dislocation density evolution and the residual stress relaxation during the annealing process.

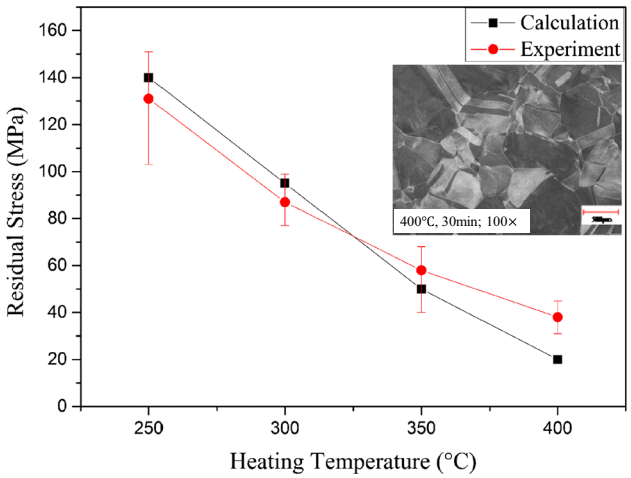


Fig. 9—Comparison of measured and calculated residual stresses during annealing at different temperatures for 30 min for the workpieces with 50 pct RR.

The stress was normalized as $\sigma_{Norm} = {}^{\sigma'}/_{\sigma_{ini}}$, where $\sigma_{ini}$ and $\sigma'$ are the initial residual stresses before annealing and residual stresses after annealing, respectively. The normalized residual stresses with different heating times from experimental measurement (symbols) and calculation (solid lines) are shown in Figure 8. The fitted hardening index $\alpha$ for each hardening level is 0.67, 0.71, and 0.73, respectively for the workpieces with 17 pct RR, 33 pct RR, and 50 pct RR. Compared with the recommended value of 0.5 for pure metals in the work-hardened state according to Frost and Ashby,[26] hardening index $\alpha$ is slightly higher due to a higher dislocation density and strong dislocation interaction but still lies in a reasonable range of 0.2 to 1.0.

As shown in Figure 8, the residual stresses dropped rapidly when the workpieces were subjected to the elevated temperature due to thermal activation. When the residual stress dropped to a relatively low level, the change rate of the residual stress was retarded. Since a low residual stress leads to a low average velocity of dislocation motion $\bar{v}$ and hence a low inelastic strain rate $\dot{\varepsilon}_{ie}$(Eqs. [1] to [5]), the residual stress is reduced slowly.

It can also be concluded that a higher initial dislocation density hindered the relaxation of residual stress when the temperature was lower than the

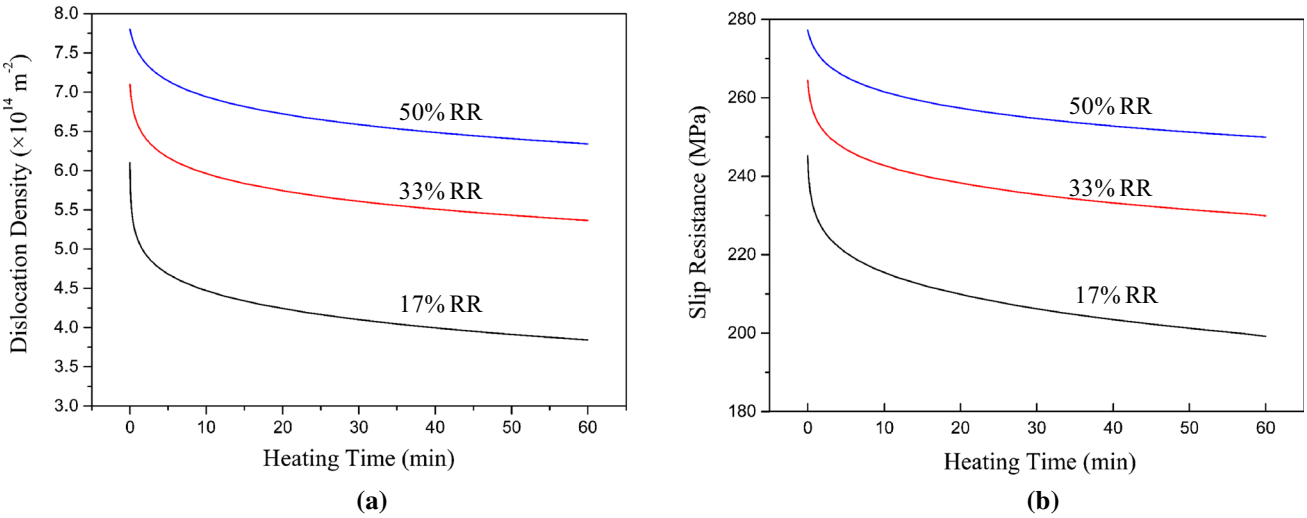


Fig. 10—Predictions of (*a*) dislocation density and (*b*) slip resistance during 300 °C annealing.

recrystallization temperature. Because $\hat{\sigma}$ is proportional to $\sqrt{\rho}$ as described in Eq. [6], a greater plastic deformation preceding the heat treatment resulted in a higher value of slip resistance $\hat{\sigma}$. In addition, as shown in Eqs. [2] to [5], [8], when the RR was increased in the experiment, the total free energy (activation energy) $\Delta F$ was increased, and hence the inelastic strain rate during stress relaxation was decreased, indicating a lower rate residual stress reduction.

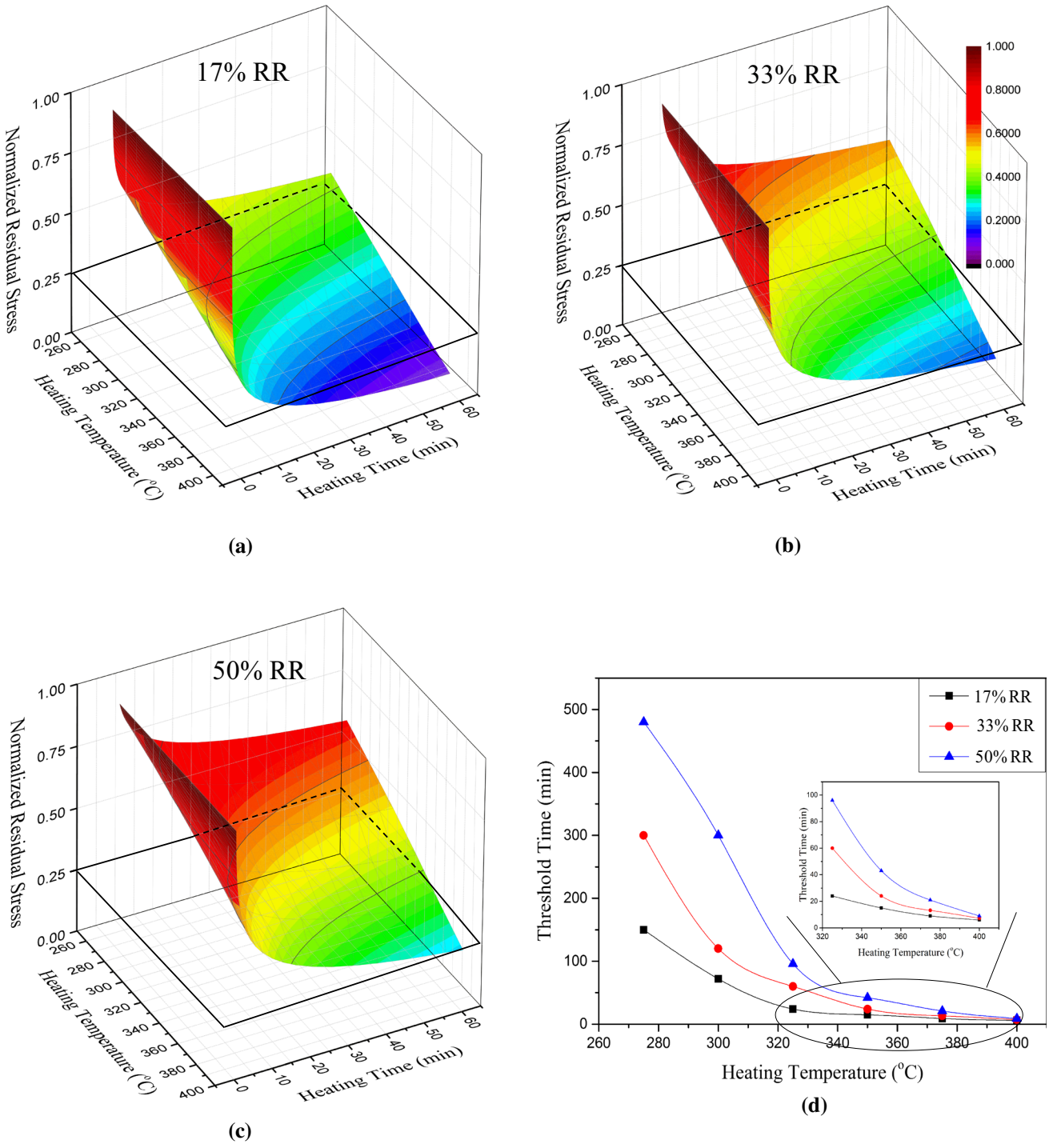


Fig. 11—Predictions of residual stresses after annealing for different workpieces with RRs of (*a*) 17 pct, (*b*) 33 pct, and (*c*) 50 pct; (*d*) relationship between heating temperatures and corresponding threshold heating times.

### C. *Model Verification*

The annealing experiments using workpieces with 50 pct RR at 250 °C, 300 °C, 350 °C and 400 °C for 30 minutes were conducted to verify the proposed model. As shown in Figure 9, with the increase of the annealing temperature, the residual stress was decreased. Based on the microstructure of the annealed workpieces at 400 °C for 30 minutes, it is deduced that there was no obvious microstructure change in the workpiece with 50 pct RR at a temperature range of 250 °C to 400 °C for 30 minutes. The calculated residual stresses after 30-minute annealing agreed well with the measured results, and the error was less than ± 20 MPa. Therefore, the theoretical model is reliable for cold-rolled copper residual stress prediction at different annealing conditions.

### D. *Predicting the Change of Residual Stress*

The dislocation density and the corresponding slip resistance $\hat{\sigma}$ in workpieces with different RRs during 300 °C annealing are predicted in Figures 10(a) and (b). During rolling, the workpieces was subjected to work hardening, and the initial dislocation densities varied from $6.1 \times 10^{14}$ to $7.8 \times 10^{14}$ $m^{-2}$ when the RR was increased from 17 to 50 pct. The dislocation density and the slip resistance were decreased rapidly firstly due to the thermal activation induced dislocation movement and annihilation, and then leveled off at a relatively low value. The reduction of the dislocation density in the workpieces with a large RR was less than that with a small RR, which has the same tendency as residual stress relaxation.

Residual stresses with different RRs were predicted at different heating temperatures during annealing as shown in Figures 11(a) to (c). A higher heating temperature could accelerate the residual stress relaxation for the workpieces with different initial hardening levels. The residual stresses were decreased more slowly in workpieces with larger RRs. Figure 11(d) shows the threshold heating time at different heating temperatures in order to decrease the residual stresses to a quarter of the initial values. For workpieces with the larger RRs, higher heating temperature and longer heating time are needed to reduce the residual stresses to the desired values. Based on Figure 11, for a given heating temperature and heating time, the residual stresses after annealing can be obtained, which provides the guidance to the selection of annealing parameters.

## V. CONCLUSIONS

A novel residual stress relaxation model, which incorporates initial dislocation density, dislocation evolution, and plastic deformation theory, has been proposed to predict the change of residual stress in annealing of cold-rolled copper. From the results of the study, the following conclusions can be drawn:

1. Initial dislocation density plays an important role in residual stress relaxation. With a higher initial dislocation density of the material, a higher heating temperature and a longer heating time are needed for thermal activation of residual stress relaxation.
2. Dislocation density is decreased in the residual stress relaxation process, which indicates that thermal softening plays a dominating role in the annealing.
3. With a higher temperature and a longer heating time, the extent of the residual stress relaxation is greater. The threshold time for residual stress relaxation with different temperatures is calculated to determine the annealing parameters.

## ACKNOWLEDGMENTS

This study was supported by the Science Challenge Project (JCKY2016212A506-0101), the National Natural Science Foundation of China (51605077), the Fundamental Research Funds for the Central Universities (DUT18LAB18), and the Science Fund for Creative Research Groups of NSFC (51621064).

## REFERENCES

1. K. Huang, W. Yang, and X. Ye: *Int. J. Mech. Sci.*, 2018, vol. 135, pp. 43–52.
2. W. Wang, H. Liu, C. Zhu, X. Du, and J. Tang: *Int. J. Mech. Sci.*, 2019, vol. 151, pp. 263–73.
3. C. Wang, C. Jiang, and V. Ji: *J. Mater. Process. Technol.*, 2017, vol. 240, pp. 98–103.
4. B.J. Foss, S. Gray, M.C. Hardy, S. Stekovic, D.S. McPhail, and B.A. Shollock: *Acta Mater.*, 2013, vol. 61 (7), pp. 2548–59.
5. Z. Wang, A.D. Stoica, D. Ma, and A.M. Beese: *Mater. Sci. Eng. A*, 2018, vol. 714, pp. 75–83.
6. J. Epp, H. Surm, T. Hirsch, and F. Hoffmann: *J. Mater. Process. Technol.*, 2011, vol. 211 (4), pp. 637–43.
7. I. Nikitin and M. Besel: *Scripta Mater.*, 2008, vol. 58 (3), pp. 239–42.
8. V.P. Radchenko, M.N. Saushkin, and V.V. Tsvetkov: *J. Appl. Mech. Technol. Phys.*, 2016, vol. 57 (3), pp. 559–68.
9. P. Dong, S. Song, and J. Zhang: *Int. J. Press. Vessel. Pip.*, 2014, vol. 122, pp. 6–14.
10. L.A. Godlewski, X. Su, T.M. Pollock, and J.E. Allison: *Metall. Mater. Trans. A*, 2013, vol. 44A (10), pp. 4809–18.
11. Z. Trojanová, P. Lukác, and K.U. Kainer: *Adv. Eng. Mater.*, 2007, vol. 9 (5), pp. 370–74.
12. K. Sherafatnia, G.H. Farrahi, and A.H. Mahmoudi: *Int. J. Mech. Sci.*, 2018, vol. 137, pp. 171–81.
13. A. Madariaga, J. Aperribay, P.J. Arrazola, J.A. Esnaola, E. Hormaetxe, A. Garay, and K. Ostolaza: *J. Mater. Eng. Perform.*, 2017, vol. 26 (8), pp. 3728–38.
14. H.D. Chandler: *Mater. Sci. Eng. A*, 2010, vol. 527 (23), pp. 6219–23.
15. B. Babu and L.E. Lindgren: *Int. J. Plast.*, 2013, vol. 50, pp. 94–108.
16. H. Wang, B. Clausen, L. Capolungo, I.J. Beyerlein, J. Wang, and C.N. Tome: *Int. J. Plast.*, 2016, vol. 79, pp. 275–92.
17. D.J. Buchanan, R. John, R.A. Brockman, and A.H. Rosenberger: *JOM*, 2010, vol. 62 (1), pp. 75–79.
18. Y.C. Lin, X.M. Chen, D.X. Wen, and M.S. Chen: *Comput. Mater. Sci.*, 2014, vol. 83, pp. 282–89.
19. F. Roters, D. Raabe, and G. Gottstein: *Acta Mater.*, 2000, vol. 48 (17), pp. 4181–89.
20. W. Blum, P. Eisenlohr, and F. Breutinger: *Metall. Mater. Trans. A*, 2002, vol. 33A (2), pp. 291–303.
21. W. Blum and P. Eisenlohr: *Mater. Sci. Eng. A*, 2009, vols. 510–511, pp. 7–13.

22. P. Eisenlohr and W. Blum: *Mater. Sci. Eng. A*, 2005, vols. 400–401, pp. 175–81.
23. S. Rahimi, M. King, and C. Dumont: *Mater. Sci. Eng. A*, 2017, vol. 708, pp. 563–73.
24. S.D. Antolovich and R.W. Armstrong: *Prog. Mater. Sci.*, 2014, vol. 59, pp. 1–160.
25. S. Curtze and V.T. Kuokkala: *Acta Mater.*, 2010, vol. 58, pp. 5129–41.
26. H.J. Frost and M.F. Ashby: *Deformation Mechanism Maps: The Plasticity and Creep of Metals and Ceramics*, Pergamon, Oxford, 1982.
27. X.G. Fan and H. Yang: *Int. J. Plast.*, 2011, vol. 27 (11), pp. 1833–52.
28. D. Kuhlmann-Wilsdorf: *Mater. Sci. Eng. A*, 1989, vol. 113, pp. 1–41.
29. U.F. Kocks and H. Mecking: *Prog. Mater. Sci.*, 2003, vol. 48 (3), pp. 171–273.
30. N. Bertin, L. Capolungo, and I.J. Beyerlein: *Int. J. Plast.*, 2013, vol. 49, pp. 119–44.
31. G.K. Williamson and R.E. Smallman: *Philos. Mag.*, 1956, vol. 1 (1), pp. 34–46.
32. G.K. Williamson and W.H. Hall: *Acta Metall.*, 1953, vol. 1, pp. 22–31.
33. M. Kazeminezhad: *Mater. Sci. Eng. A*, 2008, vol. 486, pp. 202–07.
34. L. Błaż and P. Kwapisiński: *Arch. Metall. Mater.*, 2009, vol. 54 (1), pp. 161–70.

**Publisher's Note** Springer Nature remains neutral with regard to jurisdictional claims in published maps and institutional affiliations.